Luttinger Liquid versus Charge Density Wave Behaviour in the Spinless Fermion Holstein Model

Fehske[1], Wellein[2], Hager[2], Becker[3], Sykora[3], Hübsch[3], Weiße[4], & Bishop[5]

Universities [1]Greifswald, [2]Erlangen & [3]Dresden (Germany), [4]University of New South Wales (Australia) [5]Los Alamos National Laboratory (U.S.A.)

Abstract: As a generic model describing the Luttinger-liquid (LL) to charge-density-wave (CDW) transition, we investigate the Holstein model of spinless fermions at half-filling using differnt numerical and analytical techniques. Combining exact diagonalization (ED) & kernel polynomial method we calculate exactly the photoemission and inverse photoemission spectra and analyse the electronic gap formation. Adapting a recently developed projector-based renormalization method (PRM) we monitor the phonon softening at the Peierls transition. In the metallic regime we determine the renormalised effective coupling constant and the velocity of the charge excitations by a density-matrix renormalisation group (DMRG) finite-size scaling approach. The results are used to establish the ground-state phase diagram of the model.

Motivation

Despite the many years of study of electron-phonon (EP) interaction in metallic systems, there remain fundamental problems that yet have to be resolved. Especially systems which suffer strong EP coupling in conjunction with strong electron-electron interaction are in the center of present interest. Examples are quasi-1D materials, such as MX chains, conjugated polymers or organic charge transfer complexes, where the itinerancy of the electrons strongly competes with the EP coupling which tends to establish e.g. CDW structures. Then, in particular at half-filling, Peierls insulating phases may be energetically favored over the metallic state. Many interesting questions arise not only with a view to the associated metal to insulator transition but also concerning the form of the single-particle excitation spectra well below and above the transition. At present, there is a clear need of reliable theoretical methods to tackle these problems in terms of minimal microscopic models.

Model

The perhaps simplest realization of a strongly coupled EP system, is the Holstein model of spinless fermions (HMSF):

$$\mathcal{H} = -t\sum_i (c_i^\dagger c_{i+1} + c_{i+1}^\dagger c_i) + \omega_0 \sum_i b_i^\dagger b_i - \sqrt{\varepsilon\omega_0}\sum_i (b_i^\dagger + b_i)(n_i - \tfrac{1}{2})\,. \quad (1)$$

The HMSF describes tight-binding band electrons coupled locally to harmonic dispersionless optical phonons, where t, ω_0, and g denote the electronic transfer amplitude, the phonon frequency, and the EP coupling constant, respectively. The physics of the HMSF is governed by the following parameter ratios:

$$\alpha = \omega_0/t, \quad g^2 = \varepsilon_p/\omega_0, \quad \& \quad \bar{\lambda} = \varepsilon_p/2t\,. \quad (2)$$

Despite of its simplicity the HMSF is not exactly solvable and a wide range of numerical methods has been applied in the past to map out the ground-state (GS) phase diagram in the g-ω_0-plane, in particular for the half-filled band case ($N_{el} = N/2$). There, the model most likely exhibits a transition from a LL to a charge-density wave CDW GS above a critical EP coupling strength $g_c(\omega_0) > 0$.

Metallic phase - LL scaling

DMRG results

First we present large-scale DMRG calculations, providing unbiased results for the (non-universal) LL parameters u_ρ and K_ρ. To leading order the charge velocity u_ρ and the correlation exponent K_ρ might be obtained from a finite-size scaling of the of the GS energy of a finite system $E_0(N)$ with N sites and the charge excitation gap $\Delta_{ch}(N) = E_0^{(\pm1)}(N) - E_0(N)$, where $\varepsilon_0(\infty)$ denotes the bulk GS energy density and $E_0^{\pm1}(N)$ is the GS energy with ±1 fermions away from half-filling:

$$\varepsilon_0(\infty) - (E_0(N)/N) = (\pi/3)(u_\rho/2)/N^2\,, \quad (3)$$
$$E_0^{(\pm1)}(N) - E_0(N) = \pi(u_\rho/2)/(NK_\rho)\,. \quad (4)$$

Note that these LL scaling relations were derived for the pure electronic spinless fermion model only.

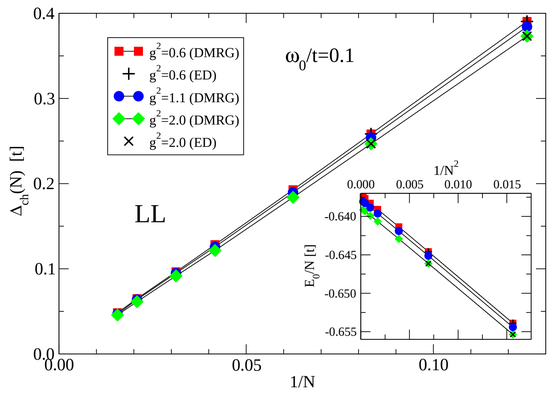

Fig.1: Finite-size scaling of the charge gap and the GS energy. ED data is included for comparison.

Figure 1 demonstrates, exemplarily for the adiabatic regime, that they also hold for the case that a finite EP coupling is included. The resulting LL parameters are given in the following table:

g^2	$\omega_0/t = 0.1$		$\omega_0/t = 10.0$	
	K_ρ	$u_\rho/2$	K_ρ	$u_\rho/2$
0.6	1.031	~ 1	~ 1	0.617
2.0	1.055	0.995	0.949	0.146
4.0	1.091	0.963	0.651	0.028

Most notably, around $\omega_0/t \sim 1$, the LL phase splits in two different regimes: For small phonon frequencies the effective fermion-fermion interaction is attractive, while it is repulsive for large frequencies. In the latter region the kinetic energy is strongly reduced and the charge carriers behave like polarons. In between, there is a transition line $K_\rho = 1$, where the LL is made up of (almost) non-interacting particles.

Peierls transition - CDW correlations

DMRG results

The LL scaling breaks down just at $g_c(\omega/t)$, i.e. at the transition to the CDW state. We found $g_c^2(\omega/t = 0.1) \simeq 7.84$ and $g_c^2(\omega/t = 10) \simeq 4.41$.

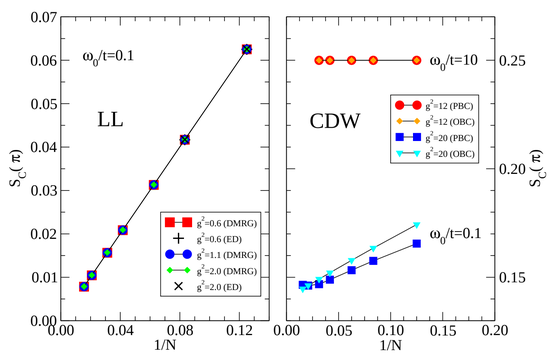

Fig.2: Scaling of the charge structure factor $S_c(\pi)$ using both periodic and open boundary conditions.

Figure 2 proves the existence of CDW long-range order above g_c. Here the charge structure factor

$$S_c(\pi) = \frac{1}{N^2}\sum_{i,j}(-1)^j\langle(n_i - \tfrac{1}{2})(n_{i+j} - \tfrac{1}{2})\rangle \quad (5)$$

scales to a finite value in the thermodynamic limit ($N \to \infty$). Simultaneously $\Delta_{ch}(\infty)$ acquires a finite value. In contrast we have $S_c(\pi) \to 0$ in the metallic regime ($g < g_c$). The CDW for strong EP coupling is connected to a Peierls distortion of the lattice, and can be classified as traditional band insulator and bipolaronic insulator in the strong-EP coupling adiabatic and anti-adiabatic regimes, respectively.

Phase diagram

DMRG and ED results

Figure 3 shows the boundary between the LL and CDW states obtained by ED and DMRG techniques:

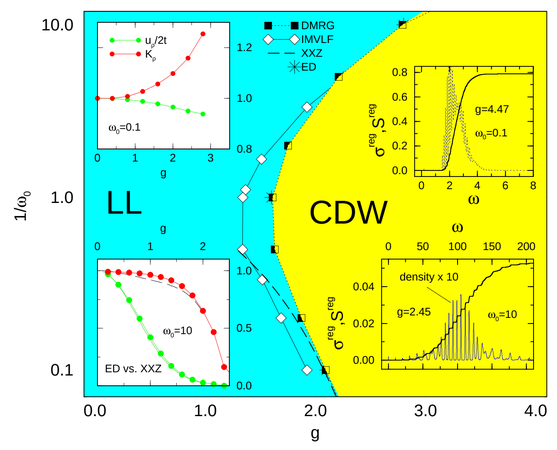

Fig.3: LL-CDW transition line in the HMSF. In the adiabatic limit ($\omega_0 \to 0$) any finite EP coupling causes a Peierls distortion. In the anti-adiabatic strong EP coupling limit ($\omega_0 \to \infty$), the HMSF can be mapped perturbatively onto the XXZ model and the metal-insulator transition is consistent with a Kosterlitz-Thouless transition at $g_c^2(\infty) \simeq 4.88$.

In Fig. 3 left insets show the LL parameters in the metallic regime. Right insets display the regular part of the optical conductivity,

$$\sigma^{\rm reg}(\omega) = \frac{\pi}{N}\sum_{m\neq0}\frac{|\langle\psi_0|\hat{j}|\psi_m\rangle|^2}{E_m - E_0}\,\delta(\omega - E_m + E_0) \quad (6)$$

with $\hat{j} = -{\rm i}et\sum_{i\sigma}(c_{i\sigma}^\dagger c_{i+1\,\sigma} - c_{i+1\,\sigma}^\dagger c_{i\sigma})$, and the integrated spectral weight $\mathcal{S}^{reg}(\omega) = \int_0^\omega d\omega' \sigma^{reg}(\omega')$ in the CDW region.

Gap formation - phonon softening

PRM & ED results

Starting point: Renormalized Hamiltonian $\mathcal{H}_\lambda = \mathcal{H}_{0,\lambda} + \mathcal{H}_{1,\lambda}$ after all excitations from $\mathcal{H}_1$ with energies larger than a cutoff λ have been eliminated

$$\mathcal{H}_{0,\lambda} = \sum_{\mathbf{k}}\varepsilon_{\mathbf{k},\lambda}\, c_{\mathbf{k}}^\dagger c_{\mathbf{k}} + \sum_{\mathbf{q}}\omega_{\mathbf{q},\lambda}\, b_{\mathbf{q}}^\dagger b_{\mathbf{q}} + E_\lambda\,, \quad (7)$$

$$\mathcal{H}_{1,\lambda} = \sum_{\mathbf{k},\mathbf{q}}\frac{g_{\mathbf{k},\mathbf{q},\lambda}}{\sqrt{N}}\,\mathbf{P}_\lambda(b_{\mathbf{q}}^\dagger c_{\mathbf{k}}^\dagger c_{\mathbf{k}+\mathbf{q}} + b_{\mathbf{q}} c_{\mathbf{k}+\mathbf{q}}^\dagger c_{\mathbf{k}})\,. \quad (8)$$

Here $\mathbf{P}_\lambda$ is a projector on excitations with energies smaller than λ.

Renormalization equations for the λ dependent parameters $\varepsilon_{\mathbf{k},\lambda}$, $\omega_{\mathbf{q},\lambda}$, and $g_{\mathbf{k},\mathbf{q},\lambda}$ are obtained by additional elimination of all excitations between λ and $(\lambda - \Delta\lambda)$ by use of the unitary transformation

$$\mathcal{H}_{(\lambda-\Delta\lambda)} = e^{X_{\lambda,\Delta\lambda}}\,\mathcal{H}_\lambda\, e^{-X_{\lambda,\Delta\lambda}}\,. \quad (9)$$

By proceeding up to $\lambda \to 0$ a diagonal Hamiltonian results: $\mathcal{H}_{\lambda\to0}$. Note that the interaction $\mathcal{H}_1$ is completely used to renormalize the parameters of $\mathcal{H}_{0,\lambda}$.

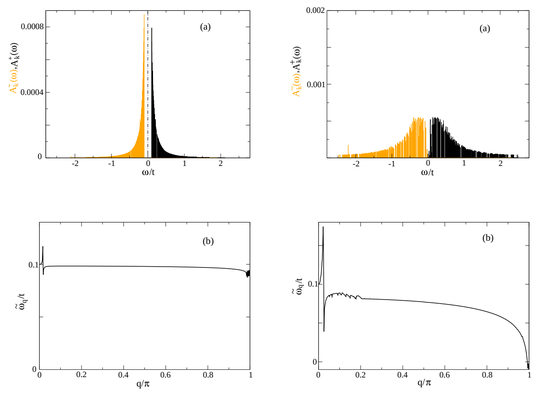

Fig. 4: (a) Electronic spectral functions $A_k^+(\omega)$ (black) and $A_k^-(\omega)$ (orange) at $k = k_F = \pi/2$. (b) Renormalized phonon dispersion $\tilde{\omega}_q$ ($\omega_0/t = 0.1$). Left (right) panels correspond to weak [$g = 1$] (almost critical [$g = 3.0$]) EP coupling. In order to integrate the renormalization equations we considered a lattice of $N = 1000$ sites.

Applying the unitary transformation to operators also the one-particle spectral functions associated with the injection of an electron with wave vector $\mathbf{k}$, $A_{\mathbf{k}}^+(\omega)$ (inverse photoemission (IPE)), and the corresponding quantity for the emission of an electron, $A_{\mathbf{k}}^-(\omega)$ (photoemission (PE)) can be evaluated:

$$A_{\mathbf{k}}^+(\omega) = \tilde{\alpha}_{\mathbf{k}}^2\,\delta(\omega - \tilde{\varepsilon}_{\mathbf{k}})(1 - \tilde{n}_{\mathbf{k}}^c) \quad (10)$$
$$+\sum_{\mathbf{q}}\tilde{\beta}_{\mathbf{k},\mathbf{q}}^2\,\delta(\omega + \tilde{\omega}_{\mathbf{q}} - \tilde{\varepsilon}_{\mathbf{k}+\mathbf{q}})\,\tilde{n}_{\mathbf{q}}^b(1 - \tilde{n}_{\mathbf{k}+\mathbf{q}}^c)$$
$$+\sum_{\mathbf{q}}\tilde{\gamma}_{\mathbf{k},\mathbf{q}}^2\,\delta(\omega - \tilde{\omega}_{\mathbf{q}} - \tilde{\varepsilon}_{\mathbf{k}-\mathbf{q}})\,(1 - \tilde{n}_{\mathbf{k}-\mathbf{q}}^c)(1 + \tilde{n}_{\mathbf{q}}^b).$$

Figure 4 shows the single-particle spectral functions and the renormalized phonon dispersion $\tilde{\omega}_q$ from the PRM approach for g-values below the critical electron phonon coupling. If $g \ll g_c$ the pole strength $\tilde{\alpha}_{k_F}^2$ of the coherent excitation is close to its maximum value of 1 (see Fig. 5). The system is in a metallic state. Due to the coupling between the phononic and the electronic degrees of freedom, $\tilde{\omega}_q$ has gained some dispersion. As g approaches the critical coupling a strong softening of the $q = \pi$ phonon is observed. The vanishing of $\tilde{\alpha}_{k_F}^2$ at g_c marks the metal-insulator transition in agreement with DMRG results.

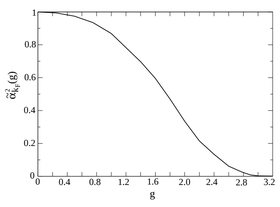

Fig. 5: Coherent pole strength $\tilde{\alpha}_{k_F}^2$ from the PRM approach as function of the EP coupling.

The ED results presented in Fig. 6 for the wave-number-resolved spectral densities,

$$A_K^\pm(\omega) = \sum_m |\langle\psi_m^{(N_{el}\pm1)}|c_K^\pm|\psi_0^{(N_{el})}\rangle|^2\,\delta[\omega \mp (E_m^{(N_{el}\pm1)} - E_0^{(N_{el})})] \quad (11)\text{–}(12)$$

($c_K^+ = c_K^\dagger$ and $c_K^- = c_K$), were obtained for an eight-site system with periodic boundary conditions.

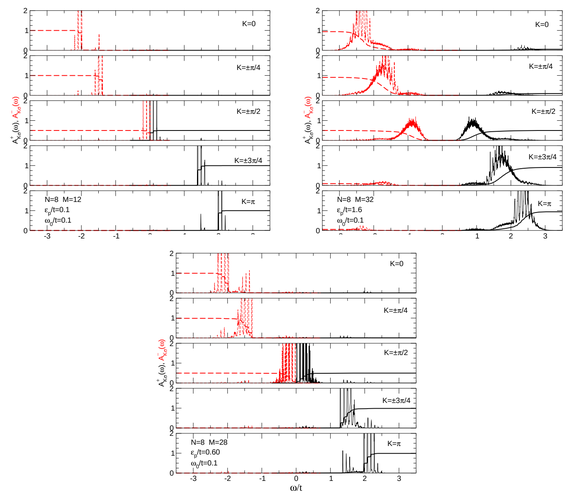

Fig. 6: Photoemission ($A_K^-(\omega)$; red lines) and inverse photoemission ($A_K^+(\omega)$; black lines) spectral functions in the adiabatic regime. For $g > g_c$ a band gap occurs, indicating massive charge excitations accompanied by multi-phonon absorption and emission processes. The system shows insulating behavior.

Conclusions

The emerging physical picture can be summarised in the following schematic phase diagram of the 1D half-filled HMSF:

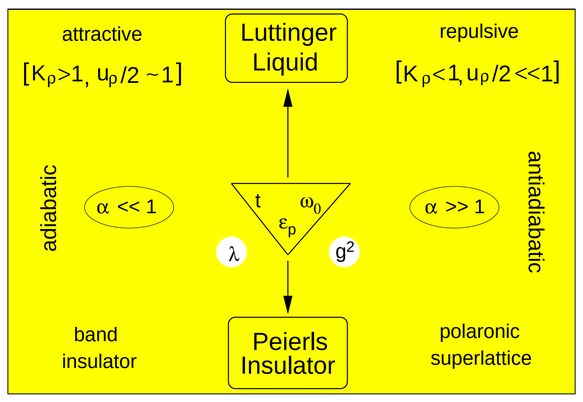

Related references:

/1/ H. Fehske *et al.*, Adv. Solid State Physics **40** , 235 (2000).
/2/ A. Weiße *et al.*, Phys. Rev. B 62 , R747 (2000).
/3/ G.Hager *et al.*, J. of Comp. Phys. **194**, 795-808 (2004).
/4/ H. Fehske *et al.*, Phys. Rev. B 69 , 165115 (2004).
/5/ S. Sykora *et al.*, cond-mat/0402184.
/6/ H. Fehske *et al.*, cond-mat/0406023.